Color-Constrained Dehazing Model

Shengdong Zhang[1,2], Yue Wu[3], Yuanjie Zhao[2], Zuomin Cheng[2], and Wenqi Ren[2*]

[1]Wuhan University   [2]SKLOIS, IIE, CAS   [3]USC Information Sciences Institute

Abstract

In this paper, we address the insufficiency of the popular atmospheric scattering model (ASM) used in the image dehazing problem. Unlike ASM assumes the global uniform atmospheric light and attenuation coefficients and thus often introduces unrealistic color after dehazing, we propose a novel dehazing model by relaxing the global uniform atmospheric assumption to local with additional color constraints to ensure more appealing and realistic dehazed results. More precisely, we make the modeling process as an optimization problem, whose cost function is composed of color constraint, local smooth of transmission map and atmospheric light. Consequently, we are able to generate more realistic dehazed images comparing to ASM, implying that deep neural networks trained with these samples could effectively learn how to dehaze images of complicated cases, especially when the global atmospheric assumption fails. Our extensive experimental studies also confirm that the proposed dehazing model outperforms the state-of-the-art methods by a noticeable margin on all three public benchmarks including HazeRD, RESIDE, and O-HAZE in terms of SSIM and PSNR.

1. Introduction

Haze is an atmospheric phenomenon whereby dust, smoke, and/or dry particles reduce the visibility of a scene and degrade image quality. As a result, only parts of the light spectrum can be received by a camera, and the camera's incoming light also inevitably blends with light rays reflected by particles. In other words, haze could severely impact the contrast and color of a captured image, and thus not only largely reduces the visibility of scenes and objects for human, but also negatively affects the performance of millions of computer vision systems all around the world, including but not limited to face recognition, text detection, object detection, pedestrian detection, action recognition, person re-identification [6, 37, 13, 19]. It is therefore an important vision task that has attracted many researchers to

Figure 1. Visual comparisons on a challenging real-world hazy example. Traditional methods (*e.g.*, DCP [10] and GridDehazeNet [18]) usually ignore the relation between the colors in dehazed result and colors in natural clean images, which leads to color distortion in dehazed results. The sky area of DCP contains noise and color distortion. The road area of GridDehazeNet contains haze. In contrast, our method effectively utilizes the relation well and maxes the prohibition of colors appeared in haze-free colors, which is able to remove color distortion and thus generate a much clearer image.

*corresponding author

study on it [39, 40, 24].

The most commonly used atmospheric scattering model (ASM) for image dehazing is a linear degradation model defined as follows [33, 34, 21]:

$$I(x) = J(x)t(x) + A(1 - t(x)), \qquad (1)$$

where $I(x)$ represents the observed hazy pixel at location x, $J(x)$ denotes the corresponding haze-free radiance to be recovered, A is the global atmospheric light, and $t(x)$ is the transmission map.

As one can see, only $I(x)$ in the ASM model (1) is known, and thus one needs extra knowledge about atmospheric light A and transmission map $t(x)$ to solve $J(x)$. Depending on whether or not estimate A and $t(x)$ directly, image dehazing method can be roughly classified into two families – prior-based and learning-based methods.

Prior-based image dehazing.   Sharp image prior-based dehazing methods require a variable clue to estimate A and $t(x)$, and thus recover $J(x)$ according to Eq. (1). For example, Based the observation that haze reduces contrast in the image, Tan [29] maximized the contrast in the dehazed image to remove haze. Based on the assumption that the shading and transmission functions are locally statistically uncorrelated, Fattal et al. [7] proposed a physically grounded method accounting for surface shading in addition to the transmission function. He et al. relied on the empirical statistics obtained by experimenting with haze-free images and proposed a dark channel prior (DCP), which indicates that at least one color channel has some pixels with very low intensities in most of the haze-free patches. Based on the DCP, He et al. proposed a method to estimate air-light and transmission map. Other authors [20, 30] have proposed dehazing methods based on DCP due to its ability for dehazing. For example, Meng et al. [20] proposed an extension to the DCP to estimate the initial transmission map and impose local transmission smoothing via $L1$-norm based contextual regularization. Based the assumption that pixels will form a line in a local haze-free image patch in the RGB space, Fattal proposed a color-line method. Based on the observation that a haze-free image can approximated with a few hundred distinct colors, Berman et al. [4] proposed a non-local dehazing method. However, all these methods ignore the relation between the pixels of dehazed result and haze-free images, which results in color distortion. As shown in Figure 1, we can see that the sky area of DCP dehazed result tend to boost noise and shown some color distortion.

Learning-based image dehazing. Recently, some learning based dehazing approaches [11, 38] directly estimates estimate A and $t(x)$, and $J(x)$ from synthetic hazy dataset. Due to the success of traditional methods [9, 29], Tang

et al. [30] proposed a method for combining the four haze-relevant features (e.g., dark channel, max contrast, hue disparity, and color attenuation) with Random Forests to estimate the transmission map. On the other hand, capitalizing on the linear relationship between the scene depth and color attenuation, Zhu et al. created a linear model for estimating scene depth and learning the model parameters through a supervised method. Due to the successful CNN application in many vision tasks [25, 26, 15, 32, 35], several CNN-based dehazing methods [5, 22] have been proposed. For example, Cai et al. [5] introduced a CNN-based method that can be applied for establishing the relationships between hazy images and transmission maps. Ren et al. improved the transmission map accuracy by adopting a multi-scale network, which first estimates a coarse-scale transmission map via a large network and refines the obtained results via a small network. On the other hand, Li et al. [11] developed a dehazing model by reformatting the scattering model and incorporating the transmission map and the atmospheric light into one new variable. Ren et al. [23] proposed a method which employs deep learning to fuse three images derived from input to generate a haze-free image. In other work, Zhang et al. [38] incorporated scattering model into a deep learning network in order to achieve end-to-end dehazing. Conditional GAN [14] has also been employed to improve the dehazing quality. First, learning-based methods learn features from synthetic hazy dataset, which is simulated using the simplified atmospheric scattering model. If the simplified atmospheric scattering model cannot hold for real hazy image, the dehazed result of learning-based methods is poor. As shown in Figure 1, the dehazed result of GridDehazeNet cannot remove haze well. In contrast, our method can achieve better dehazing with visually pleased results without any artifacts.

Despite the ASM is very popular in the image dehazing community, it suffers two major drawbacks: 1) the uniform atmospheric light A of may fail on real hazy images, especially for those are taken under complex weather conditions or scenes (see Fig. 1), and 2) it has no controls over the resulting colors in a dehazed image. In this paper, we address the both drawbacks in a single dehazing model. More precisely, we propose a generalized ASM model as follows,

$$I(x) = J(x)t(x) + A(x)(1 - t(x)) \qquad (2)$$

where we no longer force A to be a constant to represent the atmospheric light distortion for all pixels on an image, but make it an pixel location dependent coefficient $A(x)$ to better approximate the real-scenarios, and we also put explicit color-constraints that penalize the use of uncommon colors in a dehazed image.

The rest of the paper is organized as follows: Sec. 2 introduces the proposed color-constraint dehazing model;

Sec. 3 discusses the use of proposed dehazing model to generate high quality dehazed images for deep learning; and Sec. 4 compares the proposed method against various the state-of-the-arts image dehazing algorithms; and we conclude the paper in Sec 5.

2. Proposed Color-constrained Dehazing

2.1. Problem Formulation

In order to improve the ASM defined in Eq. (1), we propose a new model that penalizes unrealistic colors on the local atmospheric scattering model. The proposed model considers the color distribution, as well as local smoothing of atmospheric light and transmission map jointly.

More precisely, we restore a hazed image by optimizing the Eq. (3),

$$\min_{\bar{J}}\{-C(\bar{J})/T + \lambda_1||\nabla t||_1 + \lambda_2||\nabla A||_1\}$$
$$s.t. \ I(x) = J(x)t(x) + A(x)(1 - t(x)) \tag{3}$$

where $\bar{J}$ denotes the dehazed result, and T is the number of pixels in the hazy input image. And we explain the three terms in the target function one by one.

The first term $C(\bar{J})$ is the color constraint defined in (4)

$$C(\bar{J}) = \sum_x \log \Pr(\bar{J}(x) = [r, g, b]| \text{Real}) \tag{4}$$

where $\Pr([r, g, b]| \text{Real})$ indicates of probability seeing a dehazed $[r, g, b]$ value in the haze-free image. In practice, we estimate this distribution from 1 million haze-free images. Surprisingly, although RGB color spaces can represent 16,581,375 colors, only 2.8M colors are found in the natural haze-free images with the probability greater than 1e-5.

The second term $||\nabla t||_1$ and third $||\nabla A||_1$ denote the total variation regularization on the transmission and atmospheric light map. Please note that a local image the depth is often smooth [8] indicating that the transmission map in a nature image should also be smoothed. Moreover, the atmospheric light A is used as a map instead of a global constant. As mentioned earlier, we apply this change to alleviate the problem of uniform atmospheric light [30] in ASM. Since natural atmospheric light also changes smoothly, we also apply the total variation regularization to this term. Finally, λ_1 and λ_2 control the relative importance of the regularization for each term.

2.2. Solver

As the traditional gradient descent or other discrete optimization methods are not effective when applied to the joint optimized problem, we propose a two-step method to optimize Eq. (3), which divides the problem into solve

$\{-C(\bar{J})/T\}$ and smoothing of the transmission map and atmospheric light.

In the first step, the dehazed pixels are projected to haze-free color space, after which the transmission map and atmospheric light are smoothed. Consequently, the proposed method is an approximation of Eq. (3), making the problem easier to solve while maximizing the number of pixels projected to the haze-free color space and retaining the smoothness of the transmission map and atmospheric light. The solver components, namely hazy pixel cluster, color line cluster and smoothing of transmission map and atmospheric light, are presented below.

Hazy pixel cluster is used to reduce the computation time and ensure that the number of dehazed pixels is similar to that in the hazy domain. As objects tend to show multi-scale sizes, using one network would not yield optimal results. The dehazing result produced by CNN tends to show color inconsistencies. Consequently, hazy pixel cluster is used to capture non-local information and use it to recover the color consistently. Furthermore, hazy pixel cluster limits the number of hazy pixels being projected to large distance, which may reduce the dehazing performance. Furthermore, the pixels belonging to the same hazy pixel cluster should have similar transmission map and similar appearance in the final dehazed result.

Haze-free candidate select line cluster is used to reduce the computation time and find the candidate haze-free pixels for a special haze-free candidate select line (HCSL) cluster. Haze-line [4] has previously been used for dehazing and is a special case of haze-free candidate select line. In this work, we use haze-free candidate select line to determine which haze-free pixels can be used as the final dehazed result for a hazy pixel. As hazy image may contain one billion pixels, computing haze-free pixel candidate for each pixel is inefficient. Counter to the strategy adopted in [4], haze-free candidate select line used in the present study is determined by haze-pixel in I and the corresponding estimated haze-free pixel. Moreover, all haze-free candidate select lines are clustered to 1, 000 haze-free candidate select lines. For each HCSL cluster, we find the haze-free pixels, whereby a haze-free pixel is assigned to a HCSL cluster only if the distance to one of the HCSL cluster is smaller than the predefined threshold τ. Haze-free pixels often distribute around the distance areas from A, whereby τ adaptively depends on the distance between $I(x)$ and $\hat{J}(x)$ to allow for small intensity variations, as indicated below:

$$\tau = \frac{||\hat{J}(x) - I(x)||_1}{\lambda_0}, \tag{5}$$

where $\hat{J}$ is the network output or other results of dehazing methods. In our experiments, we find $\lambda_0 = 50$ can include possible haze-free pixels for all HCSL in a cluster. For each hazy pixel in hazy image, we find the haze-free
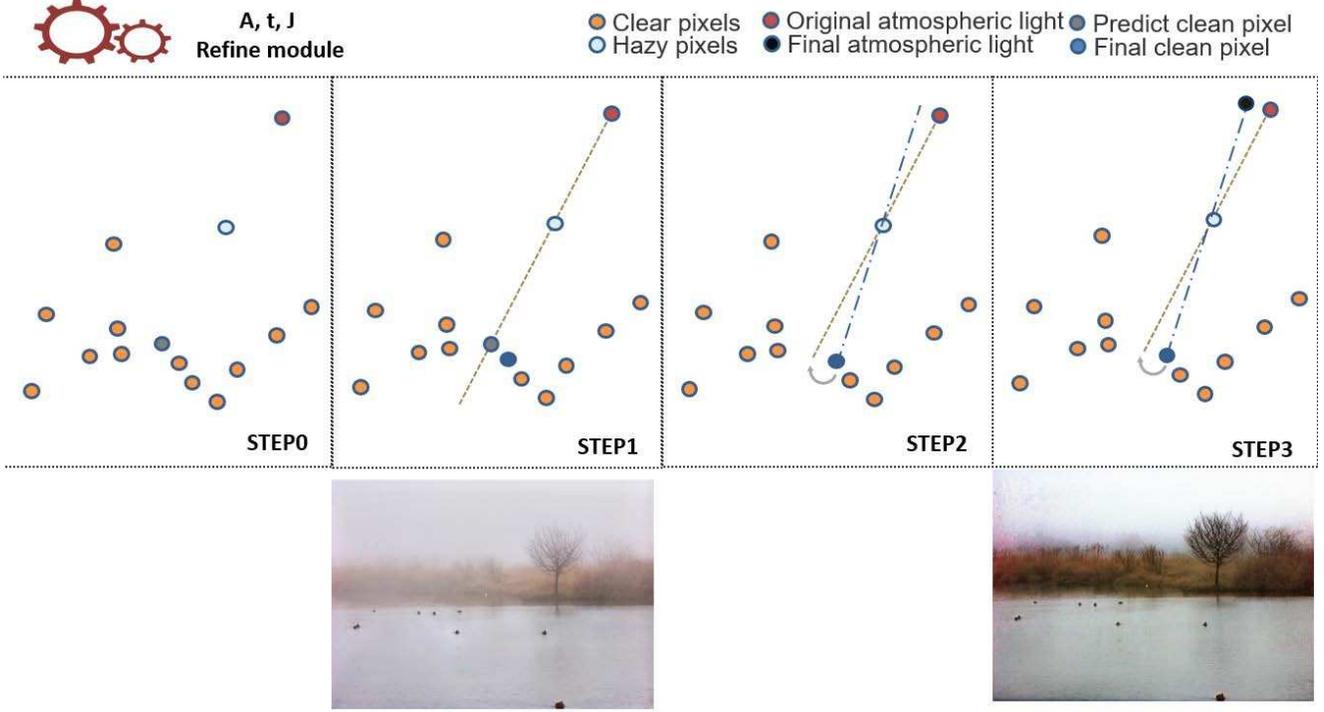
Figure 2. The steps to refine the color of dehazed pixel and atmospheric light for a hazy pixel. The first step is to find the nearest color to the line formed by the estimated haze-free pixel and hazy pixel in original hazy image. The second step is to refine the line, which will be used to find the atmospheric light. According to the new line, we find the atmospheric light, which lie at the line formed by the refined haze-free pixel and hazy pixel. Our refine module can help the dehazing methods obtain natural dehazed result.

candidate select line and then find the candidate haze-free pixels according to HCSL cluster. After obtaining the haze-free pixel, if the atmospheric light does hold for line combination of haze-free pixel and hazy pixel, we correct this situation by haze-free pixel and hazy pixel. After obtaining the atmospheric light map, we compute the transmission map. We show this process in Figure 2. The estimation of transmission map and atmospheric light is performed per-pixel, without imposing any spatial coherency conditions. As the air condition of local area in a local image patch is change smoothly, we next apply regularization on both the transmission map and atmospheric light.

Algorithm In this part, we describe the proposed algorithm in detail. Our solver assumes the A and $\hat{J}$ has obtained by deep learning-based or prior-based dehazing methods, which can be treated as a refine module for prior dehazing methods. In the first step, we project the dehazed pixel to a haze-free color space by finding the nearest color to the line formed by dehazed pixel and hazy pixel in RGB space, the result is denoted by $\hat{J}(x)$. Next, we estimate the atmospheric light using the following expression:

$$\hat{A}(x) = I(x) - (\hat{J}(x) - I(x))||I(x) - A(x)||_1. \quad (6)$$

The transmission map is subsequently calculated by apply-

ing the expression below:

$$\hat{t}(x) = \frac{||I(x) - A(x)||_1}{||\hat{J}(x) - A(x)||_1}. \quad (7)$$

After obtaining the $\hat{A}$ and $\hat{t}$, we correct the outliers by hazy pixels cluster.

Next, we smooth the transmission and atmospheric light while retaining the edge in the hazy input image by minimizing the following two functions:

$$\sum_x [\bar{A}(x) - \hat{A}(x)]^2 + \lambda_1 \sum_x \sum_{y \in N_x} \frac{[\bar{A}(x) - \hat{A}(y)]^2}{||\bar{I}(x) - \hat{I}(y)||}. \quad (8)$$

$$\sum_x [\bar{t}(x) - \hat{t}(x)]^2 + \lambda_2 \sum_x \sum_{y \in N_x} \frac{[\bar{t}(x) - \hat{t}(y)]^2}{||\bar{I}(x) - \hat{I}(y)||}. \quad (9)$$

Finally, we recover the dehazing result via the following expression:

$$J(x) = \frac{I(x) - \bar{A}(x)}{\bar{t}(x)} + \bar{A}(x) \quad (10)$$

Algorithm 1 provides a summary of all steps included in the proposed model, which can be used to refine the dehazed result of traditional or learning-based dehazing methods.

| (a) Hazy input | (b) Initial result | (c) Final airlight | (d) Final transmission | (e) Our result |

Figure 3. (a) Visual example of the model performance when applied to a challenging real-world hazy image. (b) The output of network containing haze. (c) The final atmshperic light used to recover the haze-free scene. (d) The final transmission map used to recover the haze-free scene. (e) The final dehazing result based on the original image.

Algorithm 1 The proposed single image dehazing framework.

Input: The hazy image.
Output: The final haze free image.
1: Obtain the initial dehazed result $\hat{J}$ and atmospheric light using CNN or other traditional methods.
2: Compute the haze-free candidate select line formed by hazy pixel and corresponding dehazed pixel and cluster the lines
3: Find the haze-free pixels for the haze-free candidate select line cluster
4: $error = mean(abs(\hat{J} - I))$
5: **while** $error > 0.05$ **do**
6:     Replace the dehazed pixels with a haze-free pixel nearest to the haze-free candidate select line
7:     Compute the atmospheric light A using Eq. 6
8:     Compute the transmission map according to Eq. 7
9:     Refine the atmospheric light and transmission map using hazy pixel cluster, which makes sure that pixels in same hazy pixel cluster have similar atmospheric light and transmission.
10:     Smoothen the transmission map and atmospheric light
11:     Recover the final dehazed result J according to Eq. 10
12:     $error = mean(abs(J - \hat{J}))$
13: **end while**

2.3. Discussion

Our HCSL process differs from the haze-line [4] in several aspects – First, haze-line will project the pixel on the same line to the farthest pixel, while HCSL finds the most likely one from the prior haze-free pixel distribution. Second, haze-line is determined by atmospheric light and hazy pixel, whereas HCSL is determined by hazy pixel and estimated clean pixel. Moreover, the final dehazed pixel is determined by the nearest haze-free pixel, which will help to avoid color distortion. Thirdly, as stated in [3], the boundary constraint of the transmission map (Eq. (11)) cannot hold after regularization. Our method can keep the boundary constraint well and it is based on the haze-free pixel near-
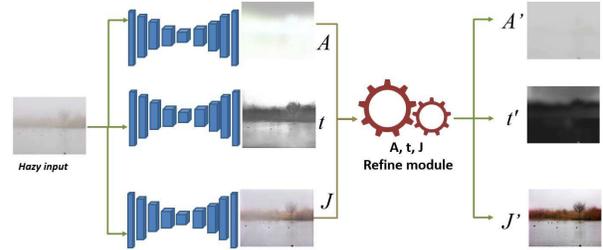

Figure 4. Architecture of the proposed networks that can be used to estimate the transmission map, atmospheric light and dehazed image. All estimators share similar architecture, while the output layer tends to vary.

est to the line formed by the hazy pixel and the predicted haze-free pixel.

$$t_{LB} = 1 - \min_{c \in \{R,G,B\}} \frac{I_c(x)}{A_c(x)} \qquad (11)$$

3. Semi-supervised Dehazing Model

The proposed model can be used to develop a semi-supervised dehazing model, which could reduce the inference time. For this purpose, we use three networks to model the three variables (atmospheric light, transmission map and haze-free image) in Eq. (3). We first train the three networks using synthetic datasets. After training the network for 10 epochs, we apply the trained model to obtain the atmospheric light, transmission map and haze-free image of natural hazy images and then refine the output of networks using the refine module. According to Eq. (3), we propose a new loss function to train the networks as shown in Eq. (12), which is composed of four terms – the reconstruction loss of hazy image, the smoothing loss of transmission map, the smoothing loss of atmospheric light and the reconstruction loss of the haze-free image $\hat{J}$.

$$\mathcal{L} = \mathcal{L}_{\text{rec}}(\bar{I}, I) + \lambda_1 ||\nabla t||_1 + \lambda_2 ||\nabla A||_1\} + \lambda_3 \mathcal{L}_{\text{rec}}(\bar{J}, \hat{J}), \qquad (12)$$

where I is the hazy image, $\hat{J}$ is the refined result of the haze-free estimating network using (3), and $\bar{I}$ can be defined as

follows:

$$\bar{I} = \bar{J}\bar{t} + \bar{A}(1 - \bar{t}), \qquad (13)$$

where $\bar{t}$ is the transmission map estimating network output, $\bar{J}$ is the haze-free estimating network output, and $\bar{A}$ is the output of atmospheric light estimating network. $\mathcal{L}_{\text{rec}}(\bar{I}, I)$ is the reconstruction loss, which can be defined as follows

$$\mathcal{L}_{\text{rec}}(\bar{I}, I) = ||\bar{I} - I||_1. \qquad (14)$$

Figure 4 illustrates the proposed training procedure of obtaining initial and refined transmission maps, atmospheric light and haze-free images. Intermediate and final dehazing results can be found Figure 3. As previously noted, conventional ASM-based CNN solutions encounters difficulties when applying to real hazy images (see Figure 4-(b)). The proposed method relies on haze-free pixels to guide the dehazing procedure and can penalize the haze-free pixels to be unrealistic, and thus mitigate the color distortion issue.

3.1. Implementation Details

The proposed model was trained on simulated hazy images using the NYU indoor dataset [27], which has been used to simulate hazy images for training CNN-based models [23, 11, 38]. During training, we use the adam optimizer with the learning rate $1e - 4$. After training our model for 10 epochs, we further fine-tune it for 40 epochs on natural hazy images [12]. When fine-tuning the model, we apply our refine module to refine the output of networks, and then training the networks using the new loss (12) on simulated hazy images and natural hazy images. We obtained haze-free pixels from haze-free images from coco dataset [16], to ensure that the colors in dehazed results produced by the dehazing process result in haze-free colors. We set $\lambda_1 = 0.01$, $\lambda_2 = 0.005$ and $\lambda_3 = 0.1$. The remaining results of the proposed method are based on semi-supervised learning. The natural hazy images (RTTS) were obtained from the RESIDE dataset [12]. We used RTTS to train our model are excluded from test hazy images.

4. Experiments

In this section, we quantitatively and qualitatively evaluate our method against eleven classic or state-of-the-art dehazing methods namely, DCP [10], BCCR [20], CAP [42], NLD [4], DehazeNet [5], MSCNN [22], AOD-Net [11], GFN [23], DCPDN [38], and PDNet [36], using both synthetic and real-world hazy images.

4.1. Quantitative Evaluation

Due to the absence of ground truths for natural hazy images, synthetic datasets have been used to evaluate the performance of dehazing methods [2, 12]. Synthetic indoor

hazy datasets are mostly used for this purpose due to the development of CNN depth estimation. High-quality depth map has been provided to synthesize hazy images [41]. However, we chose to evaluate our method on three synthetic outdoor hazy datasets to better demonstrate its performance [41, 12, 1].

Evaluations Based on the HazeRD dataset. The HazeRD dataset [41] provides natural outdoor images with high-quality depth map, which allows for simulating more realistic haze. As none of the CNN-based methods include images in HazeRD as training data, using this dataset would yield a fair comparison. As shown in Table 1, the proposed method achieves the highest PSNR and SSIM on the HazeRD testing data, and exceeds the suboptimal method (i.e., PDNet [36]) by up to 2.06 dB and 0.01 in terms of PSNR and SSIM, respectively.

Evaluations Based on the RESIDE dataset. We also evaluated the proposed model on the Synthetic Objective Testing Set (SOTS) obtained from the RESIDE dataset [12]. This test dataset contains 500 outdoor hazy images synthesized from natural outdoor images. The depth of natural images was estimated using the CNN model [17]. From Table 2, it is evident that our model again outperforms other dehazing methods in terms of the PSNR and SSIM.

Evaluation on the O-HAZE dataset. We have evaluated the proposed model on synthesized hazy image datasets, which are simulated using a simplified optical model. To further show the ability of the proposed model, we evaluate our model on the O-HAZE dataset [1], which generates haze using a professional haze machine that simulates with high fidelity real hazy conditions. As shown in Table 3, we can see that our model achieve highest performance in terms of PSNR and SSIM.

4.2. Qualitative Evaluation

Natural hazy images captured in bad weather are usually complex due to diverse lighting conditions and multiple scattering effects. We thus qualitatively evaluated the proposed method by applying it on the natural hazy images from [30]. Figure 5 shows several real-world hazy images and the dehazed results obtained by the proposed method and state-of-the-art dehazing methods [10, 31, 20, 30, 42, 28, 5, 22, 4, 38, 23]. It is evident that the traditional dehazing methods, including FVR [31] and ATM [28], fail to remove haze well and tend to produce color distortions, as shown in Figure 5(c) and 5(g). In addition, the approaches based on image priors DCP [10], BCCR [20], and NLD [4] tend to overestimate the haze concentration and thus generate darker results than those yielded by the rest methods, because priors may fail on some real hazy images (see the large white areas for DCP). It should be noted that, in some prior works [5, 22, 38], the authors developed CNN-based methods for transmission map estimation, applying

(a) Hazy input   (b) DCP   (c) FVR   (d) BCCR   (e) RF   (f) CAP   (g) ATM

(h) DehazeNet   (i) MSCNN   (j) NLD   (k) AOD-Net   (l) DCPDN   (m) GFN   (n) Our

(a) Hazy input   (b) DCP   (c) FVR   (d) BCCR   (e) RF   (f) CAP   (g) ATM

(h) DehazeNet   (i) MSCNN   (j) NLD   (k) AOD-Net   (l) DCPDN   (m) GFN   (n) Our

Figure 5. Qualitative evaluations on the real hazy images. The proposed method generates much clearer images with clearer structures and characters.
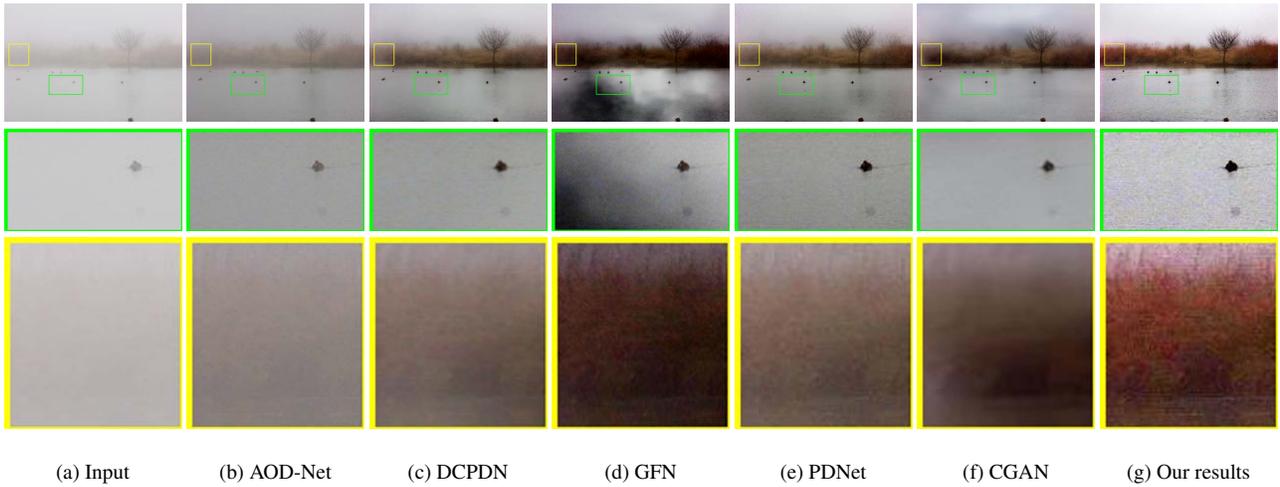
(a) Input   (b) AOD-Net   (c) DCPDN   (d) GFN   (e) PDNet   (f) CGAN   (g) Our results

Figure 6. Qualitative evaluation on the natural hazy image.

Table 1. Average PSNR/SSIM of dehazed results on the HazeRD dataset.

	DCP	BCCR	CAP	NLD	MSCNN	DehazeNet	AOD-Net	DCPDN	GFN	PDNet	Ours
PSNR	17.66	16.31	18.56	18.82	19.10	19.53	18.13	18.82	19.18	20.14	**22.20**
SSIM	0.84	0.83	0.83	0.84	0.85	0.85	0.83	0.89	0.86	0.89	**0.90**

Table 2. Average PSNR and SSIM of dehazed results on the outdoor SOTS test data from the RESIDE dataset.

	DCP	BCCR	CAP	NLD	MSCNN	DehazeNet	AOD-Net	DCPDN	GFN	PDNet	Ours
PSNR	19.13	15.08	22.27	16.85	18.64	22.46	19.06	19.93	21.55	20.89	**24.52**
SSIM	0.81	0.74	0.90	0.78	0.82	0.85	0.88	0.84	0.84	0.85	**0.92**

Table 3. Quantitative evaluation on the O-HAZE dataset [1].

	DCP	BCCR	CAP	NLD	MSCNN	DehazeNet	AOD-Net	DCPDN	GFN	PDNet	Ours
PSNR	16.59	17.44	17.62	16.61	19.07	16.21	16.72	15.62	18.30	18.52	**19.29**
SSIM	0.74	0.75	0.71	0.75	0.77	0.67	0.68	0.62	0.72	0.75	**0.78**

the conventional atmospheric model given by Eq. (1) to generate final haze-free images. However, due to the imperfectly estimated transmission maps, the final recovered images produced by these methods contain haze and generate some artifacts (see Figure 5(i) and (l)). Furthermore, the end-to-end deep learning networks proposed in [11, 23] rely on CNNs to directly estimate clear images from hazy images. However, these methods fail to generate clean images, as shown in Figure 5(k) and (m), as the assumption used to generate the training dataset is not satisfied for really hazy images. Unlike the aforementioned methods, the proposed method utilizes the information obtained from haze-free pixels, as well as alleviates the traditional atmospheric constraint given by Eq. (1). Thus, it not only removes haze well, but also reduces the potential artifacts and color distortions. It can be seen from Figure 5(n) that the images generated by our model are much clearer than those generated by other algorithms, as the proposed model can deal with dense hazy images and avoids color distortion and over-enhancement.

We further compare our method with five state-of-the-art methods [11, 38, 23, 36, 14] in Figure 6. As one can see, the end-to-end learning-based methods fail to remove haze well. For example, GFN tends to show color distortion as shown in green square. AOD-Net tends to leave haze in dehazed result. DCPDN can generate a better result than AOD-Net. However, the result of DCPDN still contains some haze. CGAN [14] and PDNet [36] cannot deal the sky area well and leave haze in yellow square area. In contrast, our model can achieve better dehazing with visually appealing results without any artifacts.

5. Conclusion

In this work, we introduced a novel color-constrained local smooth atmospheric scattering model for single image dehazing. This model is inspired by the observation that the dehazed colors should be in the haze-free color distribution. More specifically, the pixel RGB values of a dehazed image should attain the same values as they are in a haze-free image. To ensure that the dehazing result strictly follows the physics-driven scattering model for dehazing, we incorporated local smoothing into our color-constrained dehazing model. Our model overcomes the problem of uniform atmospheric light assumption and constructs relationships between dehazed results and the haze-free color distribution. We also proposed a method for solving Eq.(3). As our solver is an approximation of Eq. (3), it can be further improved. In contrast to previous methods, our method can reduce color artifacts by considering the haze-free distribution with local atmospheric scattering model. Moreover, unlike the learning-based methods, our method overcome the assumption of three equal channels of atmospheric light and uniform attenuation coefficient of the atmosphere. In

addition, we incorporated the model into a CNN framework and proposed a semi-supervised CNN-based method. Our extensive experiment results on both synthetic and real datasets demonstrated that the proposed method outperformed the state-of-the-art dehazing methods. Additional visual comparison results further confirmed the superiority of the proposed method, which produced nearly haze-free prediction with very little color distortion or dehazing artifacts.

6. Acknowledgments

References

[1] Codruta O Ancuti, Cosmin Ancuti, Radu Timofte, and Christophe De Vleeschouwer. O-haze: a dehazing benchmark with real hazy and haze-free outdoor images. In *Proceedings of the IEEE Conference on Computer Vision and Pattern Recognition Workshops*, pages 754–762, 2018. 6, 7

[2] Cosmin Ancuti, Codruta O Ancuti, and Christophe De Vleeschouwer. D-hazy: A dataset to evaluate quantitatively dehazing algorithms. In *2016 IEEE International Conference on Image Processing (ICIP)*, pages 2226–2230. IEEE, 2016. 6

[3] Dana Berman, Shai Avidan, et al. Single image dehazing using haze-lines. *TPAMI*, 2018. 5

[4] Dana Berman, Tali Treibitz, and Shai Avidan. Non-local image dehazing. In *CVPR*, 2016. 2, 3, 5, 6

[5] Bolun Cai, Xiangmin Xu, Kui Jia, Chunmei Qing, and Dacheng Tao. Dehazenet: An end-to-end system for single image haze removal. *TIP*, 25(11):5187–5198, 2016. 2, 6

[6] Xiaochun Cao, Wenqi Ren, Wangmeng Zuo, Xiaojie Guo, and Hassan Foroosh. Scene text deblurring using text-specific multiscale dictionaries. *TIP*, 24(4):1302–1314, 2015. 1

[7] Raanan Fattal. Single image dehazing. *TOG*, 27(3):72, 2008. 2

[8] Raanan Fattal. Dehazing using color-lines. *TOG*, 34(1):13, 2014. 3

[9] Kaiming He, Jian Sun, and Xiaoou Tang. Single image haze removal using dark channel prior. In *CVPR*, 2009. 2

[10] Kaiming He, Jian Sun, and Xiaoou Tang. Single image haze removal using dark channel prior. *TPAMI*, 33(12):2341–2353, 2011. 1, 6

[11] Boyi Li, Xiulian Peng, Zhangyang Wang, Jizheng Xu, and Dan Feng. An all-in-one network for dehazing and beyond. In *ICCV*, 2017. 2, 6, 8

[12] Boyi Li, Wenqi Ren, Dengpan Fu, Dacheng Tao, Dan Feng, Wenjun Zeng, and Zhangyang Wang. Benchmarking single image dehazing and beyond. *TIP*, 2018. 6

[13] Chongyi Li, Chunle Guo, Wenqi Ren, Runmin Cong, Junhui Hou, Sam Kwong, and Dacheng Tao. An underwater image enhancement benchmark dataset and beyond. *TIP*, 2020. 1

[14] Runde Li, Jinshan Pan, Zechao Li, and Jinhui Tang. Single image dehazing via conditional generative adversarial network. In *CVPR*, 2018. 2, 8

[15] Siyuan Li, Iago Breno Araujo, Wenqi Ren, Zhangyang Wang, Eric K Tokuda, Roberto Hirata Junior, Roberto Cesar-Junior, Jiawan Zhang, Xiaojie Guo, and Xiaochun Cao. Single image deraining: A comprehensive benchmark analysis. In *CVPR*, 2019. 2

[16] Tsung-Yi Lin, Michael Maire, Serge Belongie, James Hays, Pietro Perona, Deva Ramanan, Piotr Dollár, and C Lawrence Zitnick. Microsoft coco: Common objects in context. In *European conference on computer vision*, pages 740–755. Springer, 2014. 6

[17] Fayao Liu, Chunhua Shen, Guosheng Lin, and Ian Reid. Learning depth from single monocular images using deep convolutional neural fields. *TPAMI*, 38(10):2024–2039, 2016. 6

[18] Xiaohong Liu, Yongrui Ma, Zhihao Shi, and Jun Chen. Grid-dehazenet: Attention-based multi-scale network for image dehazing. In *ICCV*, October 2019. 1

[19] Yu Liu, Guanlong Zhao, Boyuan Gong, Yang Li, Ritu Raj, Niraj Goel, Satya Kesav, Sandeep Gottimukkala, Zhangyang Wang, Wenqi Ren, et al. Improved techniques for learning to dehaze and beyond: A collective study. *arXiv preprint arXiv:1807.00202*, 2018. 1

[20] Gaofeng Meng, Ying Wang, Jiangyong Duan, Shiming Xiang, and Chunhong Pan. Efficient image dehazing with boundary constraint and contextual regularization. In *ICCV*, 2013. 2, 6

[21] Wenqi Ren and Xiaochun Cao. Deep video dehazing. In *Pacific rim conference on multimedia*, 2017. 2

[22] Wenqi Ren, Si Liu, Hua Zhang, Jinshan Pan, Xiaochun Cao, and Ming-Hsuan Yang. Single image dehazing via multi-scale convolutional neural networks. In *ECCV*, 2016. 2, 6

[23] Wenqi Ren, Lin Ma, Jiawei Zhang, Jinshan Pan, Xiaochun Cao, Wei Liu, and Ming-Hsuan Yang. Gated fusion network for single image dehazing. In *CVPR*, 2018. 2, 6, 8

[24] Wenqi Ren, Jinshan Pan, Hua Zhang, Xiaochun Cao, and Ming-Hsuan Yang. Single image dehazing via multi-scale convolutional neural networks with holistic edges. *International Journal of Computer Vision*, pages 1–20, 2019. 2

[25] Wenqi Ren, Jiaolong Yang, Senyou Deng, David Wipf, Xiaochun Cao, and Xin Tong. Face video deblurring using 3d facial priors. In *ICCV*, 2019. 2

[26] Wenqi Ren, Jingang Zhang, Xiangyu Xu, Lin Ma, Xiaochun Cao, Gaofeng Meng, and Wei Liu. Deep video dehazing with semantic segmentation. *TIP*, 28(4):1895–1908, 2018. 2

[27] Nathan Silberman, Derek Hoiem, Pushmeet Kohli, and Rob Fergus. Indoor segmentation and support inference from rgbd images. In *ECCV*, 2012. 6

[28] Matan Sulami, Itamar Glatzer, Raanan Fattal, and Mike Werman. Automatic recovery of the atmospheric light in hazy images. In *ICCP*, 2014. 6

[29] Robby T Tan. Visibility in bad weather from a single image. In *CVPR*, 2008. 2

[30] Ketan Tang, Jianchao Yang, and Jue Wang. Investigating haze-relevant features in a learning framework for image dehazing. In *CVPR*, pages 2995–3000, 2014. 2, 3, 6

[31] Jean-Philippe Tarel and Nicolas Hautiere. Fast visibility restoration from a single color or gray level image. In *ICCV*, 2009. 6

[32] Yuanquan Wang, Wenqi Ren, and Huaibin Wang. Anisotropic second and fourth order diffusion models based on convolutional virtual electric field for image denoising. *Computers and Mathematics with Applications*, 66(10):1729–1742, 2013. 2

[33] Qingbo Wu, Wenqi Ren, and Xiaochun Cao. Learning interleaved cascade of shrinkage fields for joint image dehazing and denoising. *TIP*, 29:1788–1801, 2019. 2

[34] Qingbo Wu, Jingang Zhang, Wenqi Ren, Wangmeng Zuo, and Xiaochun Cao. Accurate transmission estimation for removing haze and noise from a single image. *TIP*, 2019. 2

[35] Yanyang Yan, Wenqi Ren, and Xiaochun Cao. Recolored image detection via a deep discriminative model. *TIFS*, 14(1):5–17, 2018. 2

[36] Dong Yang and Jian Sun. Proximal dehaze-net: A prior learning-based deep network for single image dehazing. In *ECCV*, pages 702–717, 2018. 6, 8

[37] Ye Yuan, Wenhan Yang, Wenqi Ren, Jiaying Liu, Walter J Scheirer, and Zhangyang Wang. Ug2+ track 2: A collective benchmark effort for evaluating and advancing image understanding in poor visibility environments. *arXiv preprint arXiv:1904.04474*, 2019. 1

[38] He Zhang and Vishal M Patel. Densely connected pyramid dehazing network. In *CVPR*, 2018. 2, 6, 8

[39] Shengdong Zhang, Fazhi He, Wenqi Ren, and Jian Yao. Joint learning of image detail and transmission map for single image dehazing. *The Visual Computer*, pages 1–12, 2018. 2

[40] Shengdong Zhang, Wenqi Ren, and Jian Yao. Feed-net: Fully end-to-end dehazing. In *ICME*, 2018. 2

[41] Yanfu Zhang, Li Ding, and Gaurav Sharma. Hazerd: an outdoor scene dataset and benchmark for single image dehazing. In *ICIP*, pages 3205–3209. IEEE, 2017. 6

[42] Qingsong Zhu, Jiaming Mai, and Ling Shao. A fast single image haze removal algorithm using color attenuation prior. *TIP*, 24(11):3522–3533, 2015. 6